On the interpretation of Mössbauer spectra of magnetic nanoparticles

Fock, Jeppe; Hansen, Mikkel Fougt; Frandsen, Cathrine; Mørup, Steen

Published in:
Journal of Magnetism and Magnetic Materials

Link to article, DOI:
10.1016/j.jmmm.2017.08.070

Publication date:
2018

Document Version
Peer reviewed version

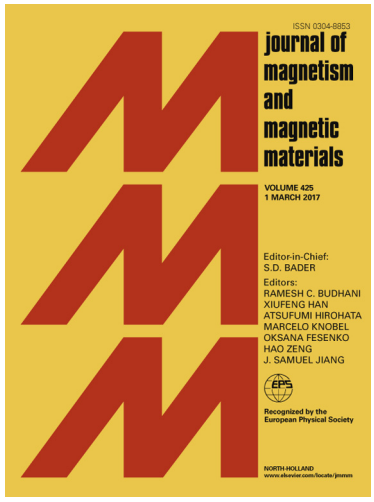

On the interpretation of Mössbauer spectra of magnetic nanoparticles

Jeppe Fock, Mikkel Fougt Hansen, Cathrine Frandsen, Steen Mørup

PII: S0304-8853(17)31457-9
DOI: http://dx.doi.org/10.1016/j.jmmm.2017.08.070
Reference: MAGMA 63104

To appear in: *Journal of Magnetism and Magnetic Materials*

Received Date: 9 May 2017
Revised Date: 26 July 2017
Accepted Date: 23 August 2017

Please cite this article as: J. Fock, M.F. Hansen, C. Frandsen, S. Mørup, On the interpretation of Mössbauer spectra of magnetic nanoparticles, *Journal of Magnetism and Magnetic Materials* (2017), doi: http://dx.doi.org/10.1016/j.jmmm.2017.08.070

On the interpretation of Mössbauer spectra of magnetic nanoparticles

Jeppe Fock[1], Mikkel Fougt Hansen[1], Cathrine Frandsen[2], and Steen Mørup[2]

[1] Department of Micro- and Nanotechnology, DTU Nanotech, Building 345B, Technical University of Denmark, DK-2800 Kongens Lyngby, Denmark.

[2] Department of Physics, Building 307, Technical University of Denmark, DK-2800 Kongens Lyngby, Denmark.

E-mail: Steen.Morup@fysik.dtu.dk

Abstract

Mössbauer spectra of magnetic nanoparticles are usually influenced by fluctuations of the direction of the magnetic hyperfine field. In samples of non-interacting particles, the superparamagnetic relaxation usually results in spectra consisting of a sum of a sextet and a doublet with a temperature dependent area ratio. This is in accordance with the exponential dependence of the superparamagnetic relaxation time on particle size and temperature in combination with the particle size distribution. An alternative interpretation of these features is a first order magnetic transition from a magnetically ordered state to a paramagnetic state. We point out that this interpretation seems not to be correct, because the doublet component has been found to transform to a magnetically split component when relatively small magnetic fields are applied, and therefore it cannot be due to a paramagnetic state. In other cases, spectra of magnetic nanoparticles consist of sextets with asymmetrically broadened lines without the presence of doublets. It has been suggested that such spectra can be explained by a multilevel model, according to which relaxation takes place between a large number of states. We point out that spectra with asymmetrically broadened lines at least in some cases rather should be explained by the influence of magnetic inter-particle interactions on the magnetic fluctuations.

1 Introduction

Magnetic nanoparticles have important applications in, for example, ferrofluids, magnetic data storage media, biomedicine, catalysis, and they are commonly found in nature, e.g. in soils, rocks and meteorites; furthermore, there are several examples of nanoparticles playing an important role in living organisms [1]. The magnetic properties of nanoparticles differ in many respects from those of bulk materials, and this has attracted much attention [1-4]. Mössbauer spectroscopy is one of the experimental techniques used extensively for studies of the magnetic properties of nanoparticles. The shape of Mössbauer spectra of magnetic nanoparticles has for decades been the subject of numerous publications, but still there seems to be conflicting interpretations. At finite temperatures the spectra are usually strongly influenced by fluctuations of the magnetization direction, such as superparamagnetic relaxation. In many cases the spectra can be described as a sum of a sextet and a doublet with relatively narrow lines and with a temperature dependent area ratio. In other cases, the spectra consist of sextets with asymmetrically broadened lines with an average hyperfine field that decreases with increasing temperature. Both types of spectra have been interpreted by use of different models. In this paper we will discuss the validity of these models.

2 The superparamagnetic relaxation time

2.1 Models for the superparamagnetic relaxation time

Since the pioneering work on nanoparticles of hematite (α-Fe_2O_3) by Kündig *et al.* [5] the standard interpretation of Mössbauer spectra consisting of a superposition of sextets and doublets with a temperature-dependent area ratio has been in terms of superparamagnetic relaxation. In the calculations of the superparamagnetic relaxation time one usually assumes uniaxial anisotropy with an anisotropy energy given by

$$E(\theta) = KV \sin^2 \theta \tag{1}$$

where K is the magnetic anisotropy constant, V is the particle volume and θ is the angle between the (sublattice) magnetization vector and the easy axis. In a ferromagnetic nanoparticle, with $\sigma = KV/k_{\mathrm{B}}T \gtrsim 2$, where k_{B} is Boltzmann's constant and T is the temperature, the superparamagnetic relaxation time is given by the Néel model as [6]

$$\tau_{\mathrm{N}} = \tau_{0\mathrm{N}} \exp(\sigma) \tag{2}$$

where

$$\tau_{0\mathrm{N}} = \frac{M_{\mathrm{s}}}{3\gamma|\gamma_{\mathrm{s}}|}\sqrt{\frac{\pi}{2KG}}\,\sigma^{-1/2} \tag{3}$$

and is on the order of $10^{-9} - 10^{-13}$ s. Here M_s[A/m] is the saturation magnetization, G [Pa] is Young's modulus, γ [s^{-1} T^{-1}] is the gyromagnetic ratio, and γ_s is the longitudinal magnetostriction constant. The Néel relaxation model is essentially an Arrhenius law describing the probability for relaxation between the two states of minimum energy at $\theta = 0°$ and $\theta = 180°$ separated by an energy barrier at $\theta = 90°$. In the literature, Eq. (2) is most often used with a *constant* value of τ_{0N}, i.e., neglecting the dependence of τ_{0N} on temperature and anisotropy as described in Eq. (3). We will refer to this case as the simplified Néel model. To distinguish the two cases, we will reserve the symbol τ_{0N} for Eq. (3) and use τ_{0N}^{C} when the value is assumed constant.

This two-level model was criticized by Brown because it does not take into account the population of low lying states within the energy wells and the diffusion of the moment orientation between them. Brown derived a Fokker-Plank differential equation, which describes the diffusion of the magnetic moment orientation by Brownian motion [7]. Brown also proposed an approximate solution for $\sigma \gtrsim 2$, which allows for a more general expression for the relaxation time as

$$\tau_B = p^{-1} R^{-1} \exp(\sigma). \tag{4}$$

Here, R is an event or attempt frequency given by

$$R^{-1} = \sigma \frac{1}{K\eta\mu_0}\left[\frac{1}{\gamma^2} + \eta^2(\mu_0 M_s)^2\right] \approx \sigma \frac{2M_s}{\gamma K} \tag{5}$$

where η is a phenomenological damping constant. Brown argued that $\gamma^{-1} \approx \eta\mu_0 M_s$ for "ordinary sized specimens", which also results in the fastest relaxation [8]. This accounts for the latter expression in Eq. (5). The value of R^{-1} is also the characteristic time for the diffusion of the magnetic moment orientation in the limit of zero anisotropy, i.e., R^{-1} is the relaxation time in the isotropic limit, $\sigma \to 0$. Again, in the literature, the value of R is often assumed constant. To distinguish this case from that in Eq. (5), we will explicitly write R^C when it is assumed that R is constant and refer to this model as the simplified Brown model. p is a population factor accounting for the influence of the population of different states within the energy well, which for $\sigma \gtrsim 2$ is given by [9]

$$p = \frac{2}{\sqrt{\pi}}\sigma^{3/2} \tag{6}$$

Note, that for a population factor of $p = 1$, Eq. (4) reduces to Néel's model, Eq. (2), with $\tau_{0N} = R^{-1}$, because it is essentially a two-level model with only the ground level populated [10].

2.2 Simple and accurate expressions for the relaxation time

The often made assumption in the literature of constant R^{-1} or $\tau_{0\mathrm{N}}$ may result in a substantial error in the determination of KV from dynamic measurements vs. temperature. For particles of the same type, it is seen from Eqs. (3) and (5) that both $\tau_{0\mathrm{N}}$ and R^{-1} depend on the particle volume and temperature. When these dependencies are included, the expressions for τ_{N} and τ_{B} show the same dependence on temperature and volume, but different dependencies on the anisotropy. Including the temperature and volume dependence of the exponential pre-factor, the relaxation time for $\sigma \gtrsim 2$ can be written as

$$\tau = C\sigma^{-1/2}\exp(\sigma) \quad (\text{valid for } \sigma \gtrsim 2) \tag{7}$$

with

$$C = \begin{cases} \frac{M_\mathrm{S}}{3\gamma|\gamma_s|}\sqrt{\frac{\pi}{2KG}} = \tau_{0\mathrm{N}}\sigma^{1/2}\text{, for Néel's model} & \text{(8a)} \\ \frac{\sqrt{\pi}}{2K\eta\mu_0}\left[\frac{1}{\gamma^2}+\eta^2(\mu_0 M_\mathrm{S})^2\right] = R^{-1}\frac{\sqrt{\pi}}{2\sigma}\text{, for Brown's model} & \text{(8b)} \end{cases}$$

In most cases, the saturation magnetization and anisotropy depend only weakly on temperature well below the Curie temperature and C can therefore to a good approximation be treated as a constant such that $R^{-1} = 2\pi^{-1/2}\,\sigma C$ for a constant C.

Eq. (7) is only valid for $\sigma \gtrsim 2$. An exact solution to Brown's differential equation, valid for all values of σ based on an infinite sum of confluent hypergeometric (Kummer) functions was found by Coffey [11,12]. A variational approach was subsequently used to find the most accurate closed-form analytical approximation [13]. Written in terms of the constant C defined in Eq. (8b), they found the relaxation time valid for all σ to

$$\tau = R^{-1}f(\sigma) = \tfrac{2}{\sqrt{\pi}}\sigma C f(\sigma) \approx C\frac{1}{\sqrt{\pi}}(\mathrm{e}^\sigma - 1)\left(\frac{1}{1+\sigma^{-1}}\sqrt{\frac{\sigma}{\pi}} + 2^{-\sigma-1}\right)^{-1}. \tag{9}$$

where $f(\sigma)$ represents an infinite sum of Kummer functions, e is Euler's number and the last expression is the closed-form analytical approximation.

We can now discuss the consequences of assuming constant values of R^{-1} and $\tau_{0\mathrm{N}}$, respectively. Fig. 1a shows the normalized relaxation times obtained assuming constant C (valid approximation), constant $\tau_{0\mathrm{N}} = \tau_{0\mathrm{N}}^{\mathrm{C}}$ (simplified Néel model) or constant $R^{-1} = (R^C)^{-1}$ (simplified Brown model).

For $\sigma > 2$, we find using Eqs. (7) and (8) that the three curves are given by $\tau/C = \sigma^{-1/2}\mathrm{e}^\sigma$ (valid approximation, dotted black curve), $\tau/\tau_{0\mathrm{N}}^{\mathrm{C}} = \mathrm{e}^\sigma$ (simplified Néel model, solid blue curve), and $\tau/(R^C)^{-1} = \frac{1}{2}\sqrt{\pi}\,\sigma^{-3/2}\mathrm{e}^\sigma$ (simplified Brown model, dotted red curve), respectively. The solid black and red curves show

the corresponding results obtained using Eq. (9) with constant C and constant $R^{-1} = (R^C)^{-1}$, respectively. A comparison of the black curves reveals that Eqs. (7) and (9) are indeed in good agreement for $\sigma > 2$.

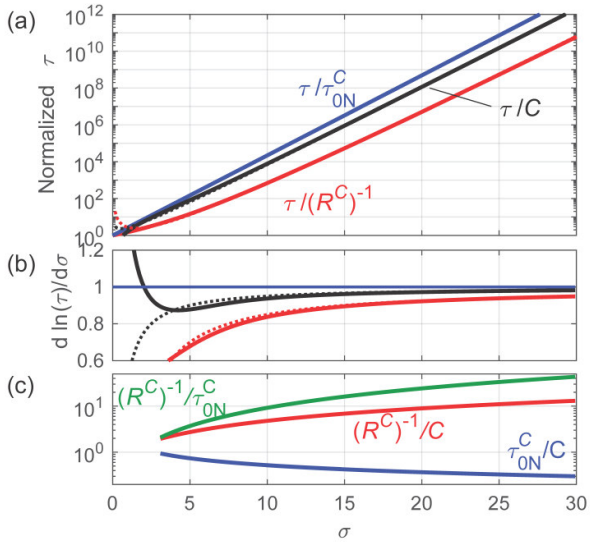

Figure 1 (a) Normalized relaxation time *vs.* $\sigma = KV/k_BT$ obtained from Eqs. (7) and (8). The black curve shows $\tau/C = \sigma^{-1/2}e^{\sigma}$ (valid approximation), the blue curve shows $\tau/\tau_{0N}^{C} = e^{\sigma}$ (simplified Néel model), and the blue curve shows $\tau/(R^C)^{-1} = \frac{1}{2}\sqrt{\pi}\,\sigma^{-3/2}e^{\sigma}$ (simplified Brown model), respectively. (b) $d(\ln\tau)/d\sigma$ vs. σ for the valid approximation (black curve), the simplified Néel model (blue curve), and the simplified Brown model (red curve). (c) Apparent values of τ_{0N}^{C}/C (blue curve) and $(R^C)^{-1}/C$ (red curve) vs. σ, Eq. (12), obtained assuming validity of the simplified Néel and Brown expressions. The green curve shows the corresponding ratio, $(R^C)^{-1}/\tau_{0N}^{C}$.

Experimentally, the relaxation time is measured as a function of temperature. Above, we have argued that Eq. (7) with a constant value of C provides a good description of the relaxation time vs. σ for $\sigma \geq 2$. Hence, the value of the KV and C obtained from fits to Eq. (7) will correctly represent the superparamagnetic relaxation for all $\sigma \geq 2$. However, in the literature, the analysis is often performed in terms of the Néel relaxation expression, Eq. (2), with a constant value τ_{0N}^{C} assumed for τ_{0N} (blue line in Fig. 1a) or in terms of the Brown relaxation expression, Eq. (4), with a constant value $(R^C)^{-1}$ assumed for R^{-1} (red line in Fig. 1a). In Fig. 1a, the blue and red curves obtained with these assumptions clearly deviate from the correct black curve. Therefore, an analysis assuming a constant value of τ_{0N} or R^{-1} will result in values of τ_{0N}^{C} or $(R^C)^{-1}$ that depend on the value of σ and differ from the correct value, C. Moreover, the values of the anisotropy constants obtained with these assumptions, termed K_N or K_B for the Néel and Brown models, will also deviate from the correct value, K. Below, we estimate the error in the determination of the anisotropy constant when using Eq. (2) or Eq. (4) with constant values of τ_{0N} and R^{-1} and relate τ_{0N}^{C} and $(R^C)^{-1}$ to C as a function of σ.

2.3 *Consequences of use of simplified Néel and Brown expressions*

The anisotropy constant can be found from the slope of $\ln(\tau)$ vs. $\frac{1}{T}$ for the different models. For $\sigma > 2$ the slope can be calculated analytically from Eqs. (2), (4) and (7) assuming constant values of $\tau_{0\mathrm{N}}$, R^{-1}, and C, respectively, as

Eq. (2) with $\tau_{0\mathrm{N}} = \tau_{0\mathrm{N}}^{\mathrm{C}}$: $$\frac{\mathrm{d}\ln\tau_{\mathrm{N}}}{\mathrm{d}\left(\frac{1}{T}\right)} = \frac{K_{\mathrm{N}}V}{k_{\mathrm{B}}} \tag{10a}$$

Eq. (4) with $R^{-1} = \left(R^{\mathrm{C}}\right)^{-1}$: $$\frac{\mathrm{d}\ln\tau_{\mathrm{B}}}{\mathrm{d}\left(\frac{1}{T}\right)} = \frac{K_{\mathrm{B}}V}{k_{\mathrm{B}}} - \frac{3T}{2} \tag{10b}$$

Eq. (7) with constant C: $$\frac{\mathrm{d}\ln\tau}{\mathrm{d}\left(\frac{1}{T}\right)} = \frac{KV}{k_{\mathrm{B}}} - \frac{T}{2} \tag{10c}$$

The slope is often constant in the range of temperatures studied in the experiments. This can be inferred from Fig. 1a where the three models by eye all appear linear for $\sigma > 5$. Figure 1b compares the slopes calculated from Eq. (9) (solid lines) with the approximations in Eq. (10) (dotted lines). We observe that Eqs. (10b) and (10c) are good approximations to the exact solution for $\sigma > 5$. Using Eq. (10), we can for $\sigma \geq 5$ relate K_{N} and K_{B} to K as

$$\frac{K_{\mathrm{N}}}{K} = \frac{\sigma_{\mathrm{N}}}{\sigma} = 1 - \frac{1}{2\sigma} \tag{11a}$$

$$\frac{K_{\mathrm{B}}}{K} = \frac{\sigma_{\mathrm{B}}}{\sigma} = 1 + \frac{1}{\sigma} \tag{11b}$$

where $\sigma_{\mathrm{N/B}} = K_{\mathrm{N/B}}V/k_{\mathrm{B}}T$. Thus, K_{N} will underestimate K and K_{B} will overestimate K. For large values of σ, K_{B} and K_{N} converge towards K.

In most cases, all of the three above models can produce fits of good quality to experimental data. However, as shown above for Néel's model with $\tau_{0\mathrm{N}} = \tau_{0\mathrm{N}}^{\mathrm{C}}$ and Brown's model with $R^{-1} = \left(R^{\mathrm{C}}\right)^{-1}$, the parameters resulting from the fits depend on the value of σ. Low values of σ are typically probed in experiments with a short observation time, such as Mössbauer spectroscopy. Large values of σ are typically probed in experiments with a long observation times, such as DC and AC magnetic susceptibility measurements.

2.4 *Correction for use of simplified Néel and Brown expressions*

To find the corresponding relations between $\tau_{0\mathrm{N}}^{\mathrm{C}}$ and C and $\tau_{0\mathrm{B}}^{\mathrm{C}}$ and C as function of σ, we insert Eqs. (11a) and (11b) in Eqs. (2) and (4), respectively, and equate the resulting expressions to Eq. (7) to obtain

$$\tau_{0\mathrm{N}}^{\mathrm{C}} = C\sigma^{-1/2}\,\mathrm{e}^{1/2} \tag{12a}$$

$$(R^{\mathrm{C}})^{-1} = 2C(\pi\sigma)^{-1/2}(\sigma+1)^{3/2}\,\mathrm{e}^{-1}. \tag{12b}$$

Figure 1c shows $\tau_{0\mathrm{N}}^{\mathrm{C}}/C$ and $(R^{\mathrm{C}})^{-1}/C$ vs. σ as well as $(R^{\mathrm{C}})^{-1}/\tau_{0\mathrm{N}}^{\mathrm{C}}$ vs. σ. From the figure, it is observed that the deviation from one increases with increasing σ and that the deviation can be more than an order of

magnitude. It is also clear that $\tau_{0\mathrm{N}}^{\mathrm{C}}$ underestimates the value of C, whereas $(R^{\mathrm{C}})^{-1}$ overestimates the value of C. Therefore, great care should be taken when comparing values of $\tau_{0\mathrm{N}}^{\mathrm{C}}$ and $(R^{\mathrm{C}})^{-1}$ obtained from such analyses.

It is also convenient to express C in terms of $\tau_{0\mathrm{N}}^{\mathrm{C}}$ and σ_{N} or $(R^{\mathrm{C}})^{-1}$ and σ_{B}. From Eqs. (11) and (12), we obtain

$$C = \tau_{0\mathrm{N}} \mathrm{e}^{-1/2} (\sigma_{\mathrm{N}} + \tfrac{1}{2})^{1/2} \tag{13a}$$

$$C = (R^{\mathrm{C}})^{-1} \tfrac{1}{2} \mathrm{e} \sqrt{\pi} (\sigma_{\mathrm{B}})^{-3/2} (\sigma_{\mathrm{B}} - 1)^{1/2} \tag{13b}$$

To be able to compare the parameters between experiments and models, parameters obtained using the above simplified and approximate Néel and Brown models can be corrected post-analysis to be of the generally correct form of Eq. (7) using the following procedure:

1) Estimate a range of σ_{N} or σ_{B} used in the experiment. Use the reported value of $\tau_{0\mathrm{N}}^{\mathrm{C}}$ or $(R^{\mathrm{C}})^{-1}$ and the interval of measurement times τ_{M} to calculate σ_{N} or σ_{B} using Eq. (2) or (4).
2) Calculate C from Eq. (13) (if in valid range of σ).

3 Mössbauer spectra with superposition of sextets and doublets

3.1 Effect of magnetic fluctuations and particle size

The shape of Mössbauer spectra in the presence of magnetic relaxation has been the subject of numerous publications since the early theoretical works by Afanas'ev and Kagan [15,16], Wickmann *et al.* [17], and Blume and Tjon [18]. Figure 2 shows theoretical spectra calculated on the basis of the two-level model by Blume and Tjon where the magnetic hyperfine field fluctuates between values of ±55 T and the quadrupole shift is 0.1 mm/s. For relaxation times well below 1 ns the spectra consist of a doublet (or a singlet if there is no quadrupole interaction). For relaxation times much longer than 1 ns, the spectra consist of sextets. In the intermediate range of relaxation times the spectra have broadened lines, where all lines of the spectrum are significantly broadened.

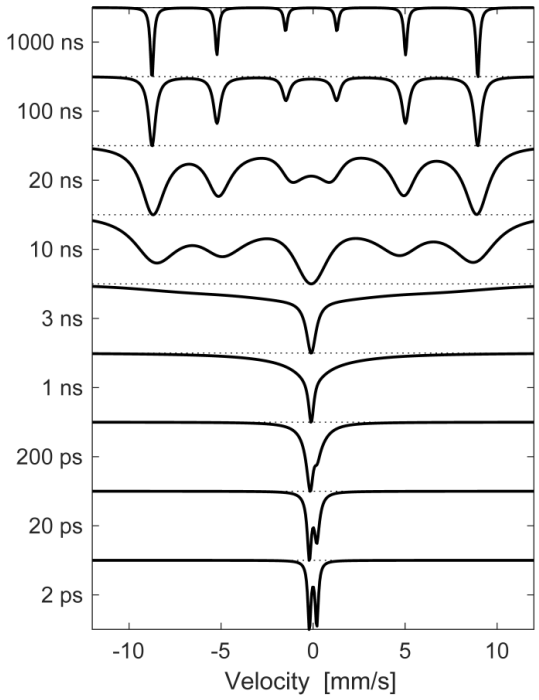

Figure 2 Theoretical Mössbauer relaxation spectra calculated on the basis of the two-level relaxation model by Blume and Tjon [18] at the indicated relaxation times with a hyperfine field switching between ±55 T. A quadrupole shift of 0.1 mm/s was assumed.

In samples of superparamagnetic particles, there is inevitably a distribution of particle sizes and magnetic anisotropy constants, resulting in a distribution of relaxation times. At a given temperature, a fraction of larger particles may have relaxation times longer than the time scale of Mössbauer spectroscopy (τ_M ~ a few nanoseconds) and contribute with a sextet component, whereas a fraction of smaller particles may have relaxation times shorter than τ_M and contribute with a doublet or singlet component. Because of the approximately exponential temperature dependence of the relaxation time and the particle size distribution, the area ratio of the two components will depend on temperature. Particles with relaxation times on the order of τ_M contribute with components with broadened lines. As an example, Fig. 3 shows Mössbauer spectra of samples of hematite nanoparticles with average diameters of 5.9 nm, 14.4 nm and 27 nm [19]. In these nanoparticles, the value of τ_{0N}^{C} was found to be on the order of 10^{-11} to 10^{-10} s using Mössbauer spectroscopy [19]. At low temperatures, the relaxation time is much longer than τ_M and the spectra consist of sextets with relatively sharp lines. The magnetic hyperfine field is slightly reduced compared to the bulk value because of fast fluctuations of the magnetization vector in directions close to the easy direction of magnetization [20-22]. For a particle with uniaxial anisotropy, the magnetic hyperfine field at low temperatures ($k_B T < 10KV$) is given by

$$B_{\mathrm{hf}}(T) \cong B_{\mathrm{hf}}(T=0)\left[1-\frac{k_{\mathrm{B}}T}{2KV}\right]. \quad (14)$$

Because of the particle size distribution, these fluctuations may lead to a temperature-dependent line broadening corresponding to a distribution of magnetic hyperfine fields. For such a distribution, the outermost lines of the magnetically split spectrum will be broadened more than the innermost lines corresponding to relative broadenings for lines 1:2:3 of 1:0.58:0.15. Thus, a signature of a magnetic hyperfine field distribution is that the outermost lines are broad whereas the innermost lines are sharp. At high temperatures, the relaxation time of the hematite particles may be much smaller than τ_M resulting in spectra consisting of quadrupole doublets with relatively narrow lines (Fig. 3). The spectra of all three samples show essentially only the presence of sextets and doublets with relatively narrow lines, and components with broadened lines due to particles with relaxation times on the order of τ_M are not clearly visible. The solid lines are fits to the Blume-Tjon model with the particle size distribution taken into account. In the fits, the model was modified to allow relaxation between plus and minus a magnetic hyperfine field given by Eq. (14) for each particle size to account for the magnetization fluctuations near the energy minima. The fits show that only a small fraction of the particles have relaxation times on the order of τ_M, i.e., only a very small fraction of the particles gives rise to broad spectra.

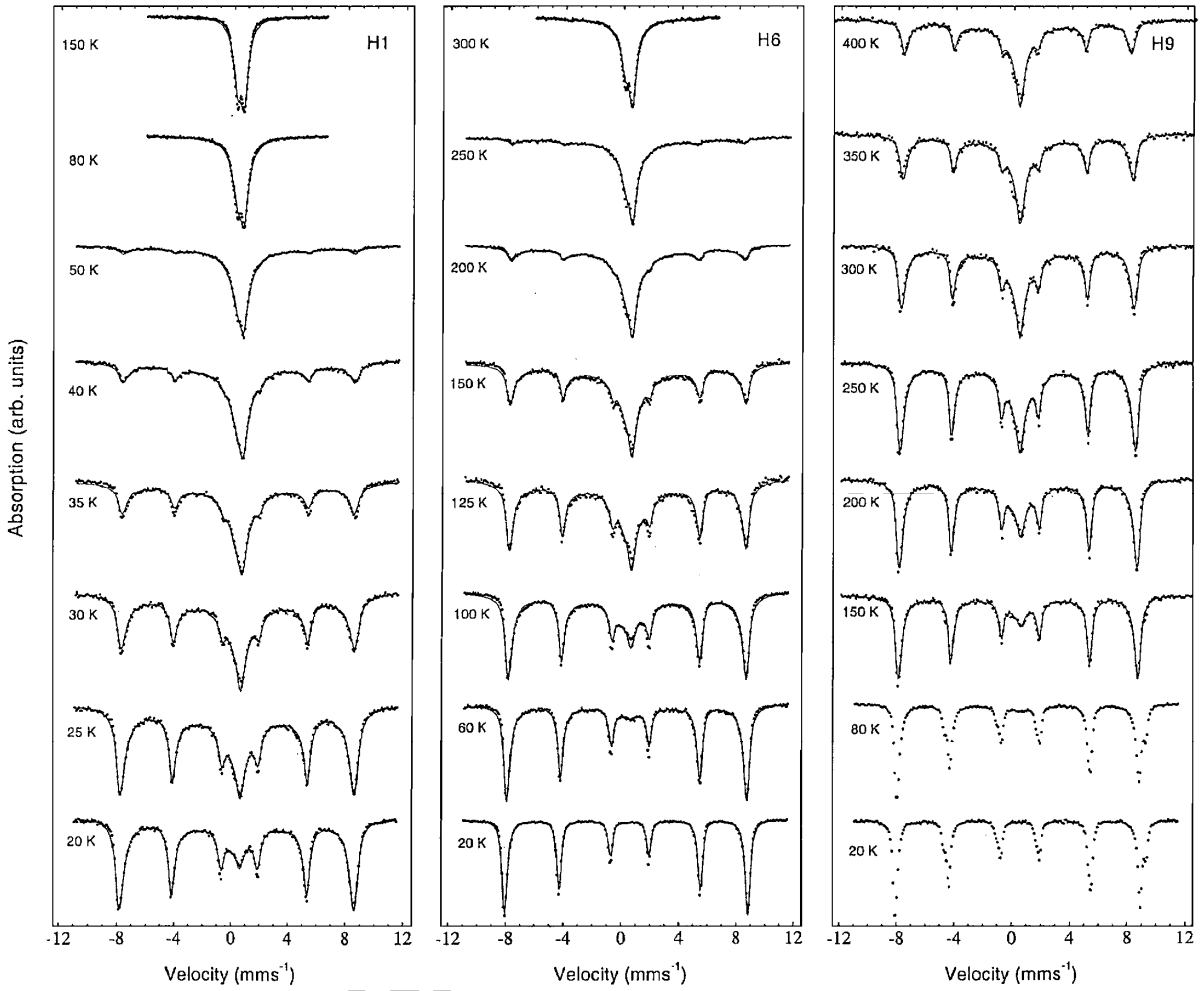

Figure 3 Mossbauer spectra of hematite nanoparticles with average diameters of 5.9 nm (H1), 14.4 nm (H6) and 27 nm (H9). The spectra were obtained at the indicated temperatures. The figure has been reproduced with permission from F. Bødker and S. Mørup, Europhys. Lett. **52**, 217 (2000) [19].

To shed further light on the connection between the value of τ_{0N}^{C}, the particle size distribution and the appearance of the resulting Mössbauer spectra vs. temperature, we first calculate the link between the temperature $T(d)$ at which particles of diameter d have a superparamagnetic relaxation time equal to τ for the simplified Néel relaxation model. Solving Eq. (2) with $\tau_{0N} = \tau_{0N}^{C}$ and $V = \frac{\pi}{6}d^3$, we obtain

$$T(d) = \frac{\pi K d^3}{6k_B \ln(\tau/\tau_{0N}^{C})}. \quad (15)$$

This expression links temperature and particle size for a given observation time. Considering Fig. 2, we next note that particles with $\tau \gtrsim 10^{-7}$ s and $\tau \lesssim 10^{-9}$ s contribute to a sharp-lined sextet and a doublet (or singlet), respectively, whereas particles with relaxation times between these values contribute with components that

are broadened by relaxation with the most significant broadening being for 3 ns $\lesssim \tau \lesssim$ 20 ns. In a more precise model, the value of $T(d)$ can be found numerically by solving Eq. (9) with a constant value of C. Figure 4 shows $T(d)$ vs. d for particles with $K = 5{\cdot}10^4$ J/m^3 calculated from Eq. (9) for three values of C. We have divided the plots in the bottom row of Fig. 4 into zones using the contours for τ = 1 ns, 3 ns, 20 ns and 100 ns, respectively. Regions of the $T(d)$ vs. d diagram where particles contribute to a sharp-lined doublet and sextet are indicated by white and black, respectively. Particles contributing with relaxation components are indicated by shades of grey where a darker shade of grey indicates that the spectra are progressively more split. Particles contributing with substantially broadened spectra at a given temperature correspond to a medium grey color. The top row shows an example of a particle size distribution, $p(d)$, which is assumed to be volume-weighted such that $p(d)\mathrm{d}d$ gives the volume fraction of particles with sizes between d and d+dd. As an example, we consider a measurement temperature T_m = 150 K for the three values of C (related to $\tau_{0\mathrm{N}}^{\mathrm{C}}$ in the simplified Néel model via Eq. (12a)) as indicated by the dashed horizontal line in the $T(d)$ vs. d plots. The parts of the particle size distribution contributing to the spectra with doublets, sextets and relaxation components at this temperature are indicated in the size distribution by the colors as described above. It is clearly observed that the fraction of the particles in the size distribution contributing with relaxation components, i.e., the grey colors in the top row of Fig. 4, becomes progressively larger for increasing values of C as the transition from white to black is broadened on the scale of particle diameters. Moreover, for C = 9 ns, it is observed that none of the particles give rise to a spectrum, which has collapsed to a sharp-lined doublet. Moreover, it is clear that a substantial fraction of the particles will contribute with components affected by relaxation. For C = 0.9 ns, only a small fraction of the particles will give rise to a collapsed spectrum. This shows that the sharp transition from a sextet to a doublet is primarily observed in particle systems with a low value of C and a comparatively broad size distribution.

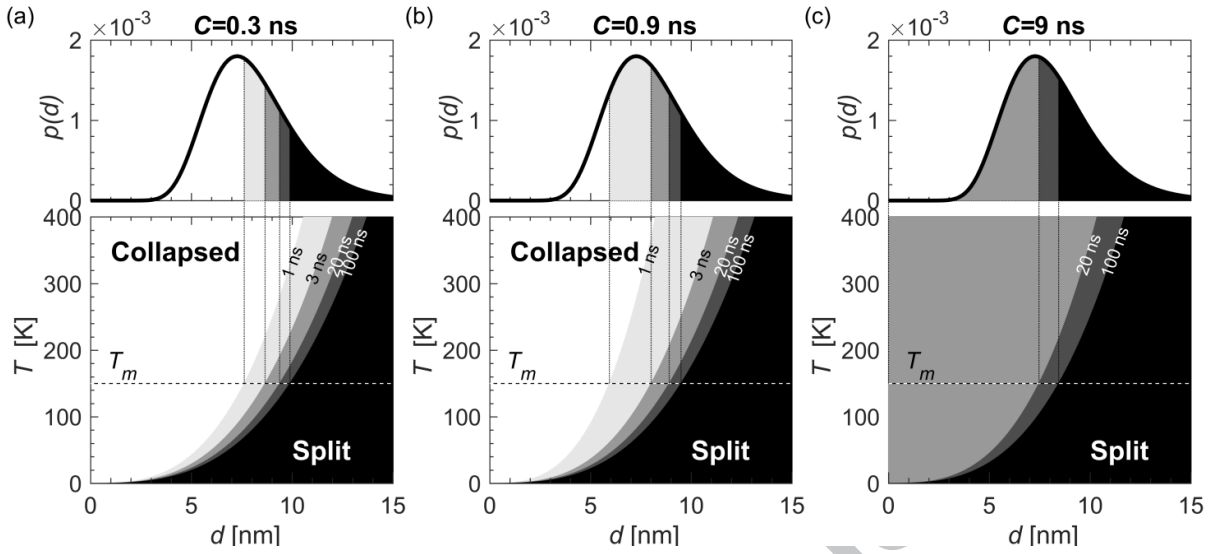

Figure 4 Bottom row: Temperature contours $T(d)$ at which a particle of diameter d has the indicated values of the superparamagnetic relaxation time τ calculated by solving Eq. (9) for the three indicated values of C. Black and white corresponds to $\tau > 10^{-7}$ s and $\tau < 10^{-9}$ s where sharp-lined sextets and singlets are observed in the Mössbauer spectra, respectively. Grey colors indicate intermediate values of τ where the Mössbauer spectra are affected by relaxation. A measuring temperature of T_m = 150 K is illustrated by the dashed horizontal line. Top row: Particle size distribution in which the distribution of relaxation times at T_m = 150 K is indicated by the different shades of grey. An anisotropy constant $K = 5 \cdot 10^4$ J/m^3 was used in the calculations.

3.2 First order magnetic phase transition?

Suzdalev *et al*. have proposed an alternative explanation of spectra such as those presented in Fig. 3 [23-28]. They obtained spectra of nanoparticles of, for example, ferrihydrite [23-25], maghemite (γ-Fe_2O_3) [24, 25] and hematite (α-Fe_2O_3) [26] showing a superposition of sextets and doublets with a temperature-dependent area ratio. They suggested that the observed transition from sextets to doublets in Mössbauer spectra of magnetic nanoparticles is not due to an onset of fast superparamagnetic relaxation, but can be explained by a first order transition from a magnetically ordered state to a paramagnetic state. The same explanation was proposed by Lyubutin *et al.* in a study of nanoparticles of $CoFe_2O_4$ [29]. Paramagnetic and superparamagnetic particles can be distinguished if Mössbauer spectra are obtained in applied magnetic fields. The magnetic energy of a magnet in an applied magnetic field is given by $E = -\boldsymbol{\mu} \cdot \boldsymbol{B}$, where $\boldsymbol{\mu}$ is the magnetic moment and $\boldsymbol{B}$ is the applied magnetic field. In a superparamagnetic nanoparticle, $\boldsymbol{\mu}$ can be on the order of hundreds or thousands of Bohr magnetons and therefore magnetic saturation occurs in relatively small applied fields. For example, a magnetic field of $B \approx 0.4$ T is required to achieve 80% of saturation for a magnetic moment of 5000 Bohr magnetons at room temperature. In a paramagnetic particle, $\boldsymbol{\mu}$ is the magnetic moment of an atom and is on the order of only a few Bohr magnetons, and therefore much larger fields are required to obtain magnetic saturation at finite temperatures. For example, a magnetic field of $B \approx 400$ T is required to achieve 80% of saturation for a magnetic moment of five Bohr magnetons at room

temperature. For atomic moments, the doublet component is only slightly affected by application of a small magnetic field. Numerous Mössbauer studies of magnetic nanoparticles have shown that the doublet usually is transformed to a sextet, when magnetic fields are applied. As an example, Figure 5 shows Mössbauer spectra of ferrihydrite particles at 80 K with various applied fields [30]. Obviously, the doublet seen at zero applied field transforms to a magnetically split spectrum, when a magnetic field is applied. Similarly, spectra of 7.5 nm maghemite transform from a doublet to a sextet at 295 K, when fields up to 0.5 T are applied [31], and the spectra of weakly ferromagnetic 15 nm hematite nanoparticles transform from a doublet to a sextet when fields on the order of 1 T are applied at 230 K [32]. The spectrum of 5 nm antiferromagnetic goethite particles consists of a doublet at 260 K, but application of a magnetic field of 6 T results in a substantial broadening, corresponding to magnetic hyperfine fields up to around 40 T [33]. We know of no examples of doublet spectra of magnetic nanoparticles that are only slightly affected by applied magnetic fields as would be expected if they were paramagnetic. The excellent quality of the fits of the spectra in Fig. 3 also shows that the experimental data are in accordance with the model for superparamagnetic relaxation (although a simple visual inspection of the spectra might suggest an abrupt transition from a sextet to a doublet). Therefore, there is no experimental evidence for a first order magnetic transition to a paramagnetic state in nanoparticles as suggested by Suzdalev *et al*. [23-28].

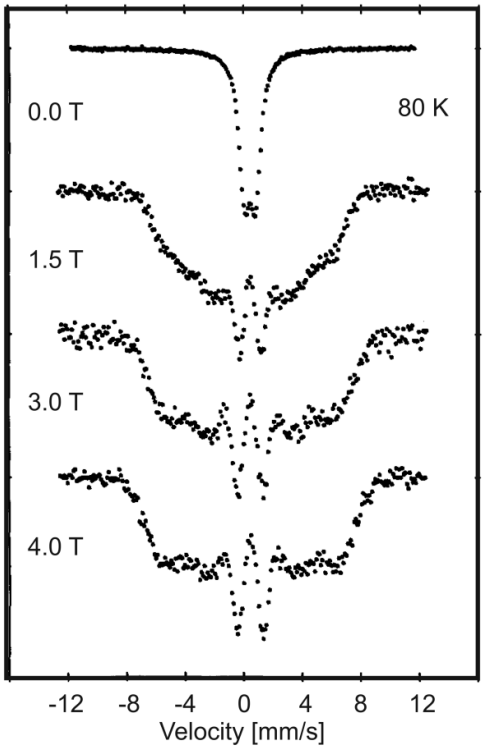

Figure 5 Mössbauer spectra of ferrihydrite nanoparticles obtained at 80 K with the indicated magnetic fields applied parallel to the gamma ray direction. The figure has been adapted with permission from M.B. Madsen, S. Mørup and C.J.W. Koch, Hyperfine Interact. **27**, 329 (1986) [30].

4 Mössbauer spectra with asymmetrically broadened lines

In several studies, Mössbauer spectra of magnetic nanoparticles have been found to be quite different from those discussed above and do not consist of a superposition of sextets and doublets at finite temperatures. Rather, they can be described as sextet components with asymmetrically broadened lines that are increasingly broadened with increasing temperature. This has been seen in, for example, several Mössbauer studies of hematite, maghemite and goethite nanoparticles, see, for example [31, 33-45]. Two competing explanations for the line shape have been made in the literature: (1) that the relaxation is influenced by inter-particle interactions; (2) that the particles are non-interacting, but the intrinsic value of C is relatively large.

4.1 Interparticle interactions - superferromagnetism

The asymmetrically broadened lines can be explained by inter-particle interactions (dipole-dipole interactions or exchange interactions), which may result in a blocking or ordering of the magnetic moments of the particles [1, 41-45]. The long-range dipole-dipole interactions can be important in samples of ferromagnetic and ferrimagnetic nanoparticles, which can have magnetic moments of up to several thousand Bohr magnetons. The magnetic moments of antiferromagnetic nanoparticles are much smaller, and dipole-

dipole interactions can therefore be considered negligible, but exchange interactions between surface atoms of particles in close proximity can be important. There are several observations showing that an increase of the inter-particle interactions can lead to a transformation of a doublet spectrum to an asymmetrically broadened sextet. Fig. 6 shows Mössbauer spectra of a frozen aqueous suspension of coated 20 nm antiferromagnetic hematite nanoparticles with negligible inter-particle interactions and of an uncoated dry sample of particles from the same fabrication batch [43]. Clearly, the increased interaction in the dried sample transforms the doublet spectra to sextets with asymmetrically broadened lines indicating an interaction-induced blocking of the magnetization fluctuations of the nanoparticles. Similar results were obtained in a study of 7 nm hematite nanoparticles [41]. In studies of ferrimagnetic nanoparticles, such as maghemite, a qualitatively similar influence of the strength of inter-particle interaction on the Mössbauer spectra has been found [31], but the effect is less pronounced, because it is difficult to avoid long-range dipole-dipole interactions, even in dilute suspensions of particles.

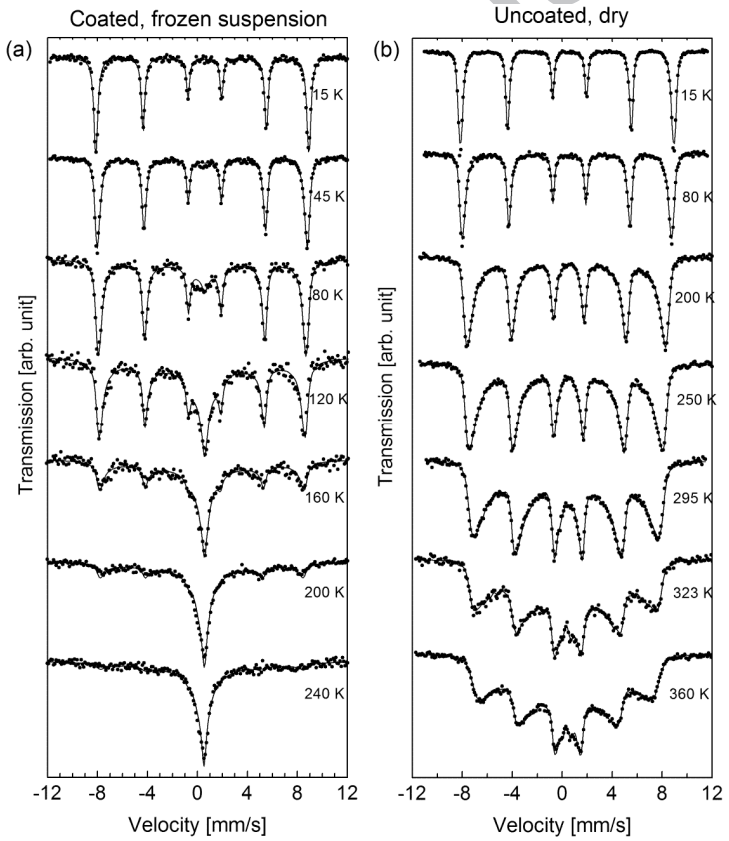

Figure 6 Mössbauer spectra of 20 nm hematite nanoparticles obtained at the indicated temperatures. (a) Particles coated with oleic acid and suspended in water in order to minimize inter-particle interactions. The solid lines are fits to the modified Blume-Tjon relaxation model. (b) Sample prepared by drying an aqueous suspension of uncoated particles. The solid lines are fits to magnetic hyperfine field distributions. The figure has been adapted with permission from M.F. Hansen, C. Bender Koch, S. Mørup, Phys. Rev. B **62**, 1124-1135 (2000) [43].

The degree of alignment of the magnetic moments can be described by an order parameter, $b(T)$. The temperature dependence of the order parameter in an assembly of strongly interacting magnetic nanoparticles has been calculated by use of a mean field theory, which has been designated the superferromagnetism model [42-45]. In a chain of interacting dipoles, a ferromagnetic ordering will be favorable [46]. In samples of, for example, interacting hematite [47] or goethite [44] nanoparticles, alignment of the sublattice magnetization vectors is also commonly seen, because of oriented attachment of the particles [44, 47]. In samples of randomly distributed ferromagnetic or ferrimagnetic nanoparticles, the moment directions will be more random such that the magnetic structure may resemble a spin glass (a super-spin glass) [4,31,48], but the term "superferromagnetism model" has often been generally used for the mean-field model for interacting nanoparticles. In this model, the magnetic energy of a nanoparticle that interacts with its neighbors is written

$$E(\theta) \approx KV \sin^2\theta - J_{\text{eff}} M_0^2(T) b(T) \cos\theta\,, \tag{16}$$

where J_{eff} is an effective interaction constant describing the magnetic interaction between a particle or grain with its neighbors, $M_0(T)$ is the sublattice magnetization and

$$b(T) = \frac{|\langle \boldsymbol{M}(T) \rangle|}{M_0(T)}. \tag{17}$$

Here, $\boldsymbol{M}(T)$ is the instantaneous value of the sublattice magnetization vector and $b(T)$ is the order parameter [41-44]. The ordering or progressive interaction-induced blocking of the magnetization should be understood broadly and it does not necessarily imply axially aligned magnetic moments as perhaps indicated by the "superferromagnetism model" naming. This naming simply reflects that the mean-field model used for the description is analogous to the Weiss model for ferromagnetic atomic systems. The temperature dependence of the order parameter can be calculated by the use of Boltzmann statistics as

$$b(T) = \frac{\int_0^\pi \exp\left(-\frac{E(\theta)}{k_{\text{B}}T}\right) \sin\theta \cos\theta \,\mathrm{d}\theta}{\int_0^\pi \exp\left(-\frac{E(\theta)}{k_{\text{B}}T}\right) \sin\theta \,\mathrm{d}\theta}. \tag{18}$$

The order parameter $b(T)$ can be found by solving numerically the coupled equations (16) and (18). At $T = 0$ K, $b(T) = 1$, but at finite temperatures the directions of the magnetization vectors fluctuate. If the magnetic fluctuations are fast compared to the time scale of Mössbauer spectroscopy, the magnetic hyperfine splitting is proportional to $b(T)$. In samples of interacting nanoparticles there will inevitably be a distribution of anisotropy energies and interaction energies. Therefore, there will be a distribution of order parameters and magnetic hyperfine fields in a sample, and this results in spectra consisting of sextets with broadened lines. This may explain the line broadening seen in the experimental spectra where the outer lines are progressively

more broadened than the inner lines, and the spectra can be fitted with a distribution of magnetic hyperfine fields. Figure 7 shows the temperature dependence of the order parameter for the median hyperfine field estimated from fits of spectra of interacting 20 nm hematite nanoparticles [43,45]. The line is a fit to the superferromagnetism model discussed above. There seems to be good agreement between the fit and the experimental data. From the fit one can estimate the interaction energy and the anisotropy energy. It was found that the estimated anisotropy energy ($K_N V/k_B \simeq 650$ K) was in excellent agreement with the value obtained from analysis of the spectra of the non-interacting particles. This strongly supports the validity of the model. The superferromagnetism model has also been successfully used to fit spectra of goethite (α-FeOOH) nanoparticles [33,44], and also in these studies it was found that the value of the anisotropy energy, estimated from the superferromagnetism model, was in accordance with that found in studies of non-interacting particles.

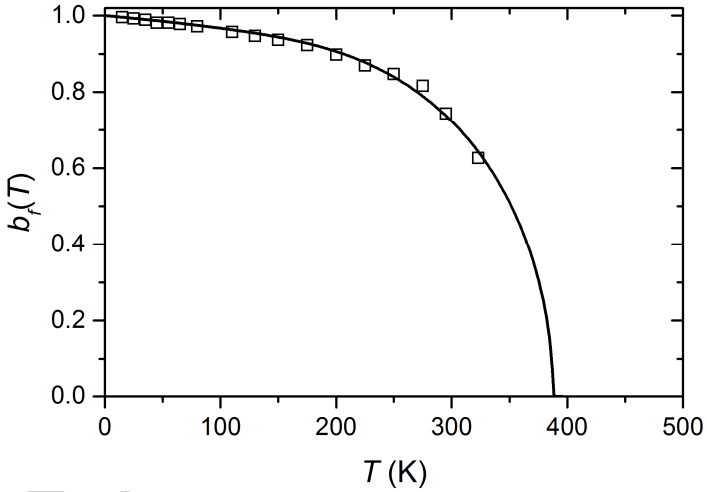

Figure 7. Temperature dependence of the median value of the order parameter for interacting 20 nm hematite nanoparticles corresponding to the spectra shown in Fig. 6b. The open squares are the experimental data and the line is a fit to the superferromagnetism model. Figure has been adapted with permission from M.F. Hansen, C. Bender Koch, S. Mørup, Phys. Rev. B **62**, 1124-1135 (2000) [43].

4.2 Multilevel relaxation modeling – results for maghemite nanoparticles

The other possible explanation of sextet components with asymmetrically broadened lines is that the value of C is relatively large. If C is on the order of 10^{-9} s, the relaxation will even at quite high temperatures not be so fast that the spectra consist of singlets or doublets with narrow lines. Spectra of this kind have been analyzed by using a multi-level model, originally proposed by Jones and Srivastava [34]. Whereas most authors have used a two-level model, i.e., a model which assumes relaxation only between the two states with minimum energy, corresponding to $\theta = 0°$ and $\theta = 180°$, the multi-level model considers also transitions between a large number of states within the two energy wells. For a particle with magnetic energy given by Eq. (1) and

with a total spin S, there are $2S+1$ states. The transition probability between adjacent states, S_z and S_z+1 is given by [34]

$$r(S_z \rightarrow S_z+1) = R[S(S+1) - S_z(S_z+1)] \quad (19)$$

where R in Eq. (19) is the previously defined attempt frequency, Eq. (5). If S is large, the multi-level model is best described by the relaxation rate described by Brown; thus if R^{-1} or $(R^{C})^{-1}$ is compared to τ_{0N}^{C}, it will be found to be larger in agreement with Fig. 1c. However, if S is small (e.g. S=1, three-level model) the moment orientation does not diffuse, and the relaxation is best described using the Néel relaxation model.

Figure 8a-c shows theoretical Mössbauer spectra calculated using three different models for a hyperfine field with a magnitude of 55 T: (1) the two-level Blume-Tjon model (blue, full lines), (2) the three-level (S=1) relaxation model (green, dotted lines), and (3) the multilevel (S=60) relaxation model (red, dashed lines). For each row in the figure all three models have the *same* superparamagnetic relaxation time as indicated to the left in the figure. The two-level Blume-Tjon model only depends on τ and is thus independent on σ and $(R^{C})^{-1}$. In contrast, the three-level model and the multilevel model depend on both σ and $(R^{C})^{-1}$. For the three-level model, the relaxation time was linked to σ and $(R^{C})^{-1}$ using the simplified Néel model, Eq. (2). For the multi-level model, the relaxation time was linked to σ and $(R^{C})^{-1}$ using the Brown model, Eq. (9). For each of these models, the value of $\sigma = \sigma(\tau)$ was found to obtain the value of τ given in the left of Fig. 8. Fig. 8d shows the corresponding values of $\sigma(\tau)$ obtained for the three-level model (green) and the multilevel model (red) for $(R^{C})^{-1}$ = 0.1 ns (circles), 5 ns (triangles) and 100 ns (squares).

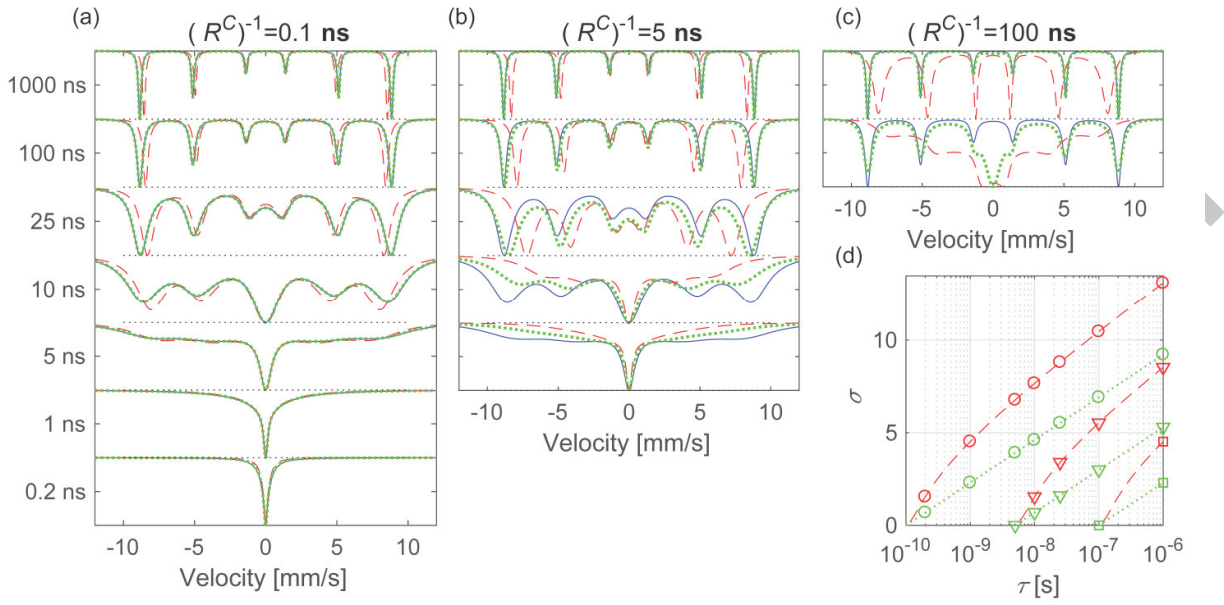

Figure 8. Theoretical Mössbauer relaxation spectra for a hyperfine field switching between ±55 T and zero quadrupole interaction at superparamagnetic relaxation time τ calculated using the Blume-Tjon model (blue, full lines), the three-level (S=1) model (green, dotted lines) and the multilevel (S=60) model (red, dashed lines). For the multilevel model, τ was calculated using the Brown model with the indicated values of R^{-1}, and for the three-level model, it was calculated using the simplified Néel model with $\tau_{0N}^{C} = R^{-1}$. In each of the models, the value of $\sigma = \sigma(\tau)$ was chosen to obtain the indicated values of τ. Panel (d) shows $\sigma(\tau)$ for the three-level model (green) and the multilevel model (red) for R^{-1}= 0.1 ns (circles), 5 ns (triangles) and 100 ns (squares).

To understand the interplay between the values of $(R^C)^{-1}$ and σ for each of the models, we first compare the shape of the calculated spectra for fixed values of R^{-1}. For the low value $(R^C)^{-1}$ =0.1 ns (Fig. 8a), it is observed that the two and three-level models resemble the shape of multi-level model, but without accounting for the collective magnetic excitations. For increasing values of $(R^C)^{-1}$ (Figs. 8b-c), the diffusion of the moment orientation becomes increasingly important and the spectra of the multi-level model deviate more from the two- and three-level models. For $(R^C)^{-1} = 100$ ns and small barrier heights, staircase-like spectra are observed.

The above observations on Fig. 8 show that the shape of relaxation Mössbauer spectra is described by R^{-1} and σ. Thus, in principle, R^{-1} and σ can directly be obtained from a fit of a single (relaxation) spectrum to the multilevel model. In a study of γ-Fe_2O_3 nanoparticles van Lierop and Ryan [35] performed fits to the multilevel model using a constant value of $(R^C)^{-1}$ as a fitting parameter at each temperature for a distribution of σ to obtain $(R^C)^{-1}$ vs. T. They observed that R^C dropped to zero at low T and reached a plateau for large T in contradiction with the linear dependence of R vs. T predicted by Eq. (5). At low temperatures, relaxation times will be long and the spectrum will be split and consequently be independent of the value of R, which can be set to zero. On the other hand, at elevated temperatures, R^{-1} should decrease.

However, if the spectrum is completely relaxed, it will be independent of R^{-1}. Thus, only fitting to partially collapsed spectra will provide reliable determination of R and C.

Landers *et al.* [40] recently used the multi-level model to fit Mössbauer spectra of 6.3 nm magnetite particles with various inter-particle separation of the magnetic nanoparticles, and found that they could be reasonably fitted assuming the constant $(R^{\mathrm{C}})^{-1} = 1.37$ ns. Using Eq. (13b), we estimate the corresponding value of C to 0.36 ns. In several papers by Chuev *et al*. on the use of the multi-level model for fits and simulations of Mössbauer spectra of magnetic nanoparticles [36-39] it was found that for $KV/\mathrm{k_B}T \lesssim 1$, the spectra were magnetically split with asymmetrically broadened lines. This implies that R^{-1} should be considerably larger than 1 ns. Table 1 summarizes the reported values of $(R^{\mathrm{C}})^{-1}$ and the corresponding estimates of C. The dependence of R on σ was not included in any of the studies although all of them used a distribution of σ in the fitting.

Table 1. Values of $(R^{\mathrm{C}})^{-1}$ (assumed constant) reported in the literature based on multilevel model fits to Mössbauer spectra of maghemite nanoparticles with various average particle diameters, d. The values of KV/k_B and $(R^{\mathrm{C}})^{-1}$ are obtained from the references and C is obtained as the mean of $C = (R^{\mathrm{C}})^{-1}\sqrt{\pi}/(2\sigma)$ for spectra showing relaxation effects. Spectra obtained at the indicated temperatures were used in the analysis.

d [nm]	$(R^{\mathrm{C}})^{-1}$ [ns]	KV/k_{B} [K]	T [K]	C [ns]	S	Reference
4.5	10-11	100	30-80	5.0	12	35
6	4-12	200	60-140	2.4	12	35
10	270	180	295 (RT)	390	-	36
4	0.2	500	80	0.34[a]	1	39
6.3	1.37	450	105-165	0.36	-	40

[a]A three-level model was used ($S = 1$). C was therefore calculated using $C = (R^{\mathrm{C}})^{-1}\sigma^{1/2}$.

4.3 Magnetization measurements on maghemite nanoparticles

In order to establish whether the spectra should be explained by a relaxation time on the order of 10^{-8} s or larger or by inter-particle interactions it is essential to have reliable estimates of C. Most experimental results were analyzed using the Néel model, Eq. (2), with a constant $\tau_{0\mathrm{N}} = \tau_{0\mathrm{N}}^{\mathrm{C}}$. The value of $\tau_{0\mathrm{N}}^{\mathrm{C}}$ was estimated in several papers on maghemite nanoparticles with negligible inter-particle interactions.

Jonsson *et al.* [49] performed measurements on a dilute frozen ferrofluid with coated maghemite nanoparticles with a particle size of 7 nm. The particle concentration by volume was 0.03%, and assuming a homogeneous dispersion of particles, the dipole-dipole interactions and exchange interactions could therefore be considered negligible. ZFC magnetic relaxation measurements were made after zero-field cooling of the sample. The sample was then gradually heated. After reaching the measurement temperature, a small field was applied and the magnetization was measured as a function of time. From these measurements they obtained $\tau_{0\mathrm{N}}^{\mathrm{C}} \simeq 0.4$ ns. The sample was also studied by AC magnetization measurements and the results were in accordance with the value of $\tau_{0\mathrm{N}}^{\mathrm{C}}$ estimated from the ZFC magnetization measurements.

Dormann *et al.* [50] studied samples of maghemite nanoparticles with different strength of the inter-particle interactions. AC magnetization measurements of a sample of 7.1 nm particles with negligible interactions showed a temperature dependence of the relaxation time in accordance with Eq. (2) and a value of $\tau_{0\mathrm{N}}^{\mathrm{C}}$ close to 10^{-10} s.

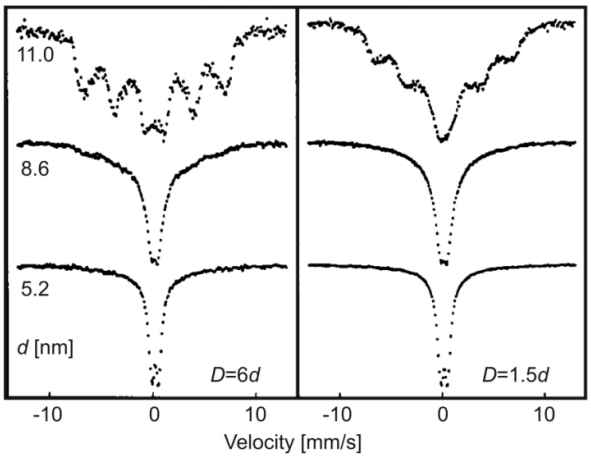

Figure 9 Room temperature Mössbauer spectra of samples of non-aggregated maghemite nanoparticles with different mean diameters, *d*, and different average center-to-center distance, *D*. The figure has been adapted with permission from Prené *et al.* Hyperfine Interactions **93**, 1409 (1994) [52].

Prené *et al.* [51, 52] prepared samples of non-aggregated maghemite nanoparticles with different mean diameter, dispersed in a polymer. Samples were made with different concentrations of particles. Figure 9 shows room temperature Mössbauer spectra of samples with mean diameters, *d*, of 5.2, 8.6 and 11.0 nm and mean center-to center distance $D = 6d$ and $D = 1.5d$ [52]. The sample with d=5.2 nm showed relatively sharp lines, indicating a relaxation time at least shorter than 1 ns. The sample with d = 8.6 nm also showed a resolved quadrupole doublet superimposed on a broad component. The latter component is presumably due to a fraction of particles with larger diameters. These spectra show unambiguously that τ and hence τ_{0N}^{C} for the studied maghemite nanoparticles was shorter than 1 ns. Only the sample with the largest particles showed a magnetically split spectrum. The relaxation time was found to decrease with increasing concentration of particles. This was explained as due to a decrease of the average energy barriers with increasing dipole interaction in samples of weakly interacting particles [53]. The relaxation slowed down only for the more concentrated samples and eventually a collective state was formed [48]. In another, more recent, study of a ferrofluid, containing 7 nm maghemite particles with negligible inter-particle interactions, AC magnetization measurements were used. In this case it was found that τ_{0N}^{C} was around 0.006 ns [54].

4.4 Discussion

Table 2 summarizes the obtained values of τ_{0N}^{C} from the literature, the interval of measurement times and the corresponding values of σ. The values of C were calculated using Eq. (13a). We observe that all values of C obtained using AC magnetization or thermo-remanent magnetization (TRM) measurements are below 1 ns.

Table 2. Literature results of magnetization measurements with measuring times τ_M on maghemite nanoparticles with diameter d. The minimum and maximum values of σ_N indicate the range of σ-values obtained by the authors using the simplified Néel model (Eq. (2) with constant $\tau_{0N} = \tau_{0N}^C$). The values of C were estimated using Eq. (13a).

d [nm]	Methods	τ_M	$\sigma_{N,min}$	$\sigma_{N,max}$	τ_{0N}^C [ns]	C [ns]	Reference
6.3	TRM	~1 s - 3600s	~23	31	0.08	0.26(4)	40
~7	ZFC	1 s-1000s	22	29	~0.4[a]	1.2(2)	49
	ACS	50 µs -1 ms	11	17	~0.4[a]	0.9(1)	
7.1	ACS	16 µs-16 ms	12	19	0.1	0.24(5)	50
7	ACS	16 µs-16 ms	15	22	0.006[b]	0.016(2)	54

[a]Obtained using the center of reported range of values. [b]Obtained using $\tau_{0N}^C = 1/(2\pi f_0)$ assuming that the authors reported f_0 rather than $\omega_0 = 1/\tau_0$.

The C-values obtained using the multi-level model of Mössbauer spectra (Table 1) are in some cases higher [35] or much higher than [36] than the value of C-values obtained from magnetization measurements in Table 2. The expression for the superparamagnetic relaxation time, Eq. (7), with a constant value of C was in Section 2.2 found to be a good representation of the exact relaxation time for $\sigma > 2$. Therefore, for non-interacting particles of the same type, the C-values estimated in Tables 1 and 2 are expected to be valid representations of the superparamagnetic relaxation time in the entire investigated temperature range. It is therefore valid to compare the values of C obtained from analyses of Mössbauer spectra in Table 1 with the corresponding values obtained from magnetization measurements in Table 2.

The C-values generally appear to be in the range 0.2-1 ns. Of the literature results, the analysis based on Ref. [36] in Table 1 yielded a value of C that was exceedingly high. Ref. [35] reported results corresponding to a C-value of 2-5 ns and Ref. [49] reported a C-value of 1.2 ns. Although good fits of the multilevel model to Mössbauer spectra were obtained in Ref. [35], the comparison to the C-values in Tables 1 and 2 suggests that these samples were influenced by interparticle interactions. This may also be the case (but to a lesser extent) for the sample studied in Ref. [49]. Ref. [54] reported results corresponding to a very low C-value of 0.016 ns. The origin of this low value is unknown.

In summary, it is clear that the multilevel model can fit spectra that are influenced by interparticle interactions, and that these spectra have a larger C value compared to free particles analyzed by other methods. The multilevel model does not explicitly describe interparticle interactions. Therefore, great care should be taken to ensure that samples are not subject to interparticle interactions as the validity of the resulting parameters is otherwise questionable. It would also be greatly beneficial to perform the analysis

using Eq. (7) with a constant C and hence use the σ-dependent value of R^{-1} given by Eq. (8b) rather than assuming that it is constant.

5. Conclusions

We have given a short review of the models for superparamagnetic relaxation in nanoparticles and the validity of the commonly used approximations to the exact values of the relaxation times. We showed that the use of the simplified Néel and Brown models may lead to deviations of the estimated parameters by up to about one order of magnitude compared to the exact values. We especially discussed the interpretation of Mössbauer spectra of magnetic nanoparticles. Often the spectra consist of a superposition of sextets and doublets with a temperature-dependent area ratio, and such spectra are usually explained by the influence of superparamagnetic relaxation. However, it has also been suggested that they may be explained by a first order magnetic transition from a magnetically ordered state to a paramagnetic state. We showed that this interpretation is not correct, because it is not in accordance with the magnetic field dependence of the spectra.

Many Mössbauer studies of, for example, maghemite nanoparticles show magnetically split spectra with asymmetrically broadened lines. Such spectra have in several cases been analyzed by using a multi-level model for non-interacting particles with an intrinsic value of $\tau_{0\mathrm{N}}^{\mathrm{C}}$ on the order of 1 ns or larger. This model can give reasonably good fits to the spectra. However, several studies of maghemite nanoparticles with negligible inter-particle interactions have shown that $\tau_{0\mathrm{N}}^{\mathrm{C}}$ is shorter than 1 ns. Because of this discrepancy, it seems that some of the parameters, estimated from fits with the multi-level model, may not be correct. Magnetic interactions between nanoparticles can have a significant influence on the relaxation, and can also lead to Mössbauer spectra with asymmetrically broadened lines. We suggest that some of the Mössbauer spectra, which have been analyzed by use of the multi-level model for non-interacting particles, should rather be analyzed by use of models that take into account the influence of inter-particle interactions on the relaxation.

Acknowledgements

Financial support from EU FP7 Grant No. 604448-NanoMag is gratefully acknowledged.

References

1. S. Mørup, M.F. Hansen and C. Frandsen in *Comprehensive Nanoscience and Technology, Vol. 2*, Eds. D. Andrews, G. Scholes and G. Wiederrecht, Elsevier (2011) 437.
2. J.L. Dormann, D. Fiorani and E. Tronc, *Adv. Chem. Phys*., **98**, 283 (1997).

3. X. Battle and A. Labarta, *J. Phys. D: Applied Physics*, **35**, R15 (2002).
4. S. Bedanta and W. Kleemann, *J. Phys. D: Appl. Phys*. **42**, 013001 (2009).
5. W. Kündig, H. Bömmel, G. Constabaris and R.H. Lindquist *Phys. Rev.* **142**, 327 (1966).
6. L. Néel, Ann. *Geophys*. **5**, 99 (1949).
7. W.F. Brown, *Phys. Rev.* **130,** 1677 (1963).
8. Brown W F, *J. Appl. Phys.* **30** S130 (1959).
9. Jones, D.H, *Hyperfine Interact.* **47-48**, 289–297. (1989)
10. W.T. Coffey, Y.P. Kalmykov, *J. Appl. Phys.* 112, 121301 (2012)
11. W.T. Coffey, D.S.F. Crothers, Y.P. Kalmykov, E.S. Massawe, J.T Waldron, *J. Magn. Magn. Mater.* **127**, L254–L260. (1993);
12. W.T. Coffey, D.S.F. Crothers, Y.P. Kalmykov, E.S. Massawe, J.T Waldron, *Phys. Rev. E* **49**, 1869–1882.(1994)
13. P.J. Cregg, D.S.F. Crothers, A.W. Wickstead, *J. Mol. Liq.* **114**, 97–104 (2004).
14. W.T. Coffey, P.J. Cregg, D.S.F. Crothers, J.T. Waldron, A.W. Wickstead, *J. Magn. Magn. Mater.* **131**, L301–L303. (1994)
15. A.M. Afanas'ev and Y. Kagan, *Zh. Eksp. Teor. Fiz.* **45**, 1660 (1963) [*Sov. Phys. JETP* **18**, 1139 (1964)].
16. Y. Kagan and A.M. Afanas'ev, *Zh. Eksp. Teor. Fiz.* **47**, 1108 (1964) [*Sov. Phys. JETP* **20**, 743 (1965)].
17. H.H. Wickman, M.P. Klein and D.A. Shirley, *Phys. Rev.* **152**, 345 (1966).
18. M. Blume and J.A. Tjon, *Phys. Rev.* **165**, 446 (1968).
19. F. Bødker and S. Mørup, *Europhys. Lett.* **52**, 217 (2000).
20. S. Mørup and H. Topsøe, *Appl. Phys.* **11**, 63 (1976).
21. S. Mørup, *J. Magn. Magn. Mater.* **37**, 39 (1983).
22. S. Mørup, C. Frandsen and M.F. Hansen, *Beilstein J. Nanotechnol.* **1**, 48 (2010).
23. I.P. Suzdalev, V.N. Buravtsev, V.K. Imshennik, Yu.V. Maksimov, V.V. Matveev, S.V. Novichikhin, A.X. Trautwein and H. Winkler, *Z. Phys. D* **37**, 55 (1996).
24. I.P. Suzdalev, *Russian Journal of Inorganic Chemistry* **54**, 2068 (2009).
25. I.P. Suzdalev and Yu. V. Maksimov, *Hyperfine Interact.* **189**, 73 (2009).
26. I.P. Suzdalev, *Russian Journal of General Chemistry* **53**, 576 (2010).
27. I.P. Suzdalev, Yu. V. Maksimov, V.K. Imshennik, S.V. Novichikhin, M.I. Ivanovskaya, D.A. Kotikov, V.V. Pan'kov and Yu. Lyubina, *Nanotechnologies in Russia*, **5**, 817 (2010).
28. I.P. Suzdalev, Yu. Maksimov, V.N. Buravtsev, V.K. Imshennik, S.V. Novichihin, V.V. Matveev and I.S. Lyubutin, *Russian Journal of Physical Chemistry B* **6**, 163 (2012).

29. I.S. Lyubutin, S.S. Starchikov, N.E. Gervits, N. Yu. Korotkov, T.V. Dmitrieva, Chung-Ron Lin, Yaw-Teng Tseng, Kun-Yauh Shih, Jiann-Shing Lee and Cheng-Chien Wang, *J. Magn. Magn. Mater.* **415**, 13 (2016).
30. M.B. Madsen, S. Mørup and C.J.W. Koch, *Hyperfine Interact.* **27**, 329 (1986).
31. S. Mørup, F. Bødker, P.V. Hendriksen and S. Linderoth, *Phys. Rev. B* **52**, 287 (1995).
32. F. Bødker, M.F. Hansen, C.B. Koch, K. Lefmann and S. Mørup, *Phys. Rev. B* **61**, 6826 (2000).
33. E. Brok, C. Frandsen, D.E. Madsen, H. Jacobsen, J.O. Birk, K. Lefmann, J. Bendix, K.S. Pedersen, C.B. Boothroyd, A.A. Bethe, G.G. Simoni and S. Mørup, *J. Phys. D: Appl. Phys*. **47**, 365003 (2014).
34. D.H. Jones and K.K.P. Srivastava, *Phys. Rev. B* **34**, 7542 (1986).
35. J. van Lierop and D.H. Ryan, *Phys. Rev. B* **63**, 064406 (2001).
36. M.A. Chuev, V.M. Cherepanov and M.A. Polikarpov, *JETP Letters* **92**, 21 (2010).
37. M.A. Chuev, *J. Phys.: Condens. Matter* **23**, 426003 (2011).
38. M.A. Chuev, *Journal of Experimental and Theoretical Physics*, **114**, 609 (2012).
39. M.A. Chuev, V.M. Cherepanov and M.A. Polikarpov, *Doklady Physics* **55**, 6 (2010).
40. J. Landers, F. Stromberg, M. Darbandi, C. Schöpper, W. Keune and H. Wende*, J. Phys.: Condens. Matter* **27**, 026002 (2015).
41. C. Frandsen and S. Mørup*, J. Magn. Magn. Mater.* **266**, 36 (2003).
42. S. Mørup, M.B. Madsen, J. Franck, J. Villadsen, and C.J.W. Koch*, J. Magn. Magn. Mater.* **40**, 163 (1983).
43. M.F. Hansen, C. B. Koch and S. Mørup*, Phys. Rev. B* **62**, 1124 (2000).
44. D.E. Madsen, L. Cervera-Gontard, T. Kasama, R.E. Dunin-Borkowski, C.B. Koch, M.F. Hansen, C. Frandsen and S. Mørup*, J. Phys.: Condens. Matter* **21**, 016007 (2009).
45. S. Mørup, M.F. Hansen and C. Frandsen, Beilstein *J. Nanotechnol*. **1**, 182 (2010).
46. M. Varon, M. Beleggia, T. Kasama, R.J. Harrison, R.E. Dunin-Borkowski, V.F. Puntes and C. Frandsen, *Sci. Rep.* **3**, 1234 (2013).
47. C. Frandsen, C.R.H. Bahl, B. Lebech, K. Lefmann, L. Theil Kuhn, L. Keller, N.H. Andersen, M. v. Zimmermann, E. Johnson, S.N. Klausen and S. Mørup, *Phys. Rev. B* **72**, 214406 (2005).
48. S. Mørup*, Europhys. Lett.* **28**, 671 (1994).
49. T. Jonsson, T. Mattsson, P. Nordblad and P. Svedlindh, *J. Magn. Magn. Mater*. **168**, 269 (1997).
50. J.L. Dormann, F. D'Orazio, F. Lucari, E. Tronc, P. Prené, J.P. Jolivet, D. Fiorani, R. Cherkaoui and M. Noguès*, Phys. Rev. B* **53**, 14291 (1996).
51. P. Prené, E. Tronc, J.P. Jolivet, J. Livage, R. Cherkaoui, M. Noguès, J.L. Dormann and D. Fiorani, *IEEE Trans. Magn.,* **29**, 2658 (1993).

52. P. Prené, E. Tronc, J.P. Jolivet, J. Livage, R. Cherkaoui, M. Noguès and J.L. Dormann, *Hyperfine Interact.* **93**, 1409 (1994).
53. S. Mørup and E. Tronc, *Phys. Rev. Lett.* **72**, 3278 (1994).
54. K.L. Pisane, E.C. Despeaux and M.S. Seehra, *J. Magn. Magn. Mater.* **384**, 148 (2015).

Expressions for the superparamagnetic relaxation time of magnetic nanoparticles are reviewed.

Consequences of using the simple Néel and Brown expressions with constant pre-factor are evaluated.

The interpretation of Mössbauer spectra of iron oxide nanoparticles with asymmetrically broadened lines is discussed.

Relaxation times of weakly/non-interacting maghemite particles reported in the literature are compared.

We argue that spectra with broadened lines in some cases are due to particle interactions.